DEPARTMENT OF PHYSICS
UNIVERSITY OF JYVÄSKYLÄ
RESEARCH REPORT No. 17/2009

SIMULATIONS OF THE STRUCTURE AND RHEOLOGY OF WET WEBS

BY
PASI MIETTINEN

Academic Dissertation
for the Degree of
Doctor of Philosophy

To be presented, by permission of the
Faculty of Mathematics and Science
of the University of Jyväskylä,
for public examination in FYS1 of the
University of Jyväskylä on December 15th, 2009
at 12 o'clock

Nummela, Finland
November 2009

Preface

The studies reviewed in this thesis have been carried out during the years 2003-2008 in Espoo (Oy Keskuslaboratorio, KCL), at the University of Wisconsin in Madison, and in Nummela, Finland. I express my gratitude to Professor Jussi Timonen and Dr. Kaarlo Niskanen, and my supervisor Dr. Jukka Ketoja for an interesting research topic and guidance.

I would like to express my gratitude to Professor Daniel J. Klingenberg for letting me use the simulation code developed in his group, and for support and guidance during and after my visit at the University of Wisconsin-Madison. Financial support from KCL and the Finnish Cultural Foundation, and computing resources of the Center for Scientific Computing (CSC) Finland, are gratefully acknowledged.

Finally, I wish to thank all those people at KCL, VTT and Metso Paper, who made contributions to this thesis. Most of all I wish to thank my wife Anu and my daughter Kirsti for support, patience, and for being there.

Nummela, November 2009

Pasi Miettinen

Abstract

In this Thesis we modified a recently introduced model for fiber suspensions to be applicable to wet fiber networks so as to analyze by computer simulations their structural and rheological properties. These properties were compared, under tensile loading in particular, to those of wet and dry paper. The model used operated at the fiber level, where the dynamics of fiber motion were determined by fiber stiffness and fiber-fiber interactions such as friction and adhesive forces. Water surface tension, inter-fiber contact area, and moisture content all contributed to the latter force.

The tensile strength of wet fiber networks could be described in terms of a very simple function of adhesion-force magnitude, number of inter-fiber contacts, friction coefficient, and network grammage. Relaxation of the tensile force as simulated for model networks was found to compare well with experimental results for wet paper, and the force was found to decrease proportional to logarithmic time. Relaxation rate in the model networks and in wet paper was found to be higher than in dry paper for which previous results are available.

In the simulations the permanent deformation that appeared after relaxation was, however, clearly higher than what was measured in wet paper. We suggest that this difference arises because, in the model networks, all the contact points between fibers were frictional, while in real wet paper there may also appear some chemical bonding between fibers.

Results of analytical models and computer simulations for the number of fiber-fiber contacts in compressed and stretched fiber networks were compared. When the majority of fibers lay parallel to the xy plane, the analytical and numerical predictions for the number of contacts were in good agreement both for compressed and stretched networks. However, in flocculated and stretched networks the strain was mainly concentrated between flocs that remained largely intact during straining. The non-uniform strain in this case means that mean-field approach does not work for wet flocculated networks.

Simulation of tri-axial deformation of model networks showed that the lateral network-contraction ratio (Poisson ratio) was nearly constant for very small strains as expected for a linear regime. There after it increased with increasing applied strain and sample length. For very large strains it leveled off to a constant value depending on the sample length. Simulations also captured the experimentally observed behavior for paper thickness during straining: The thickness of the network decreased or increased during stretching depending on fiber stiffness.

List of publications

I. P.P.J MIETTINEN, J.A. KETOJA, AND D.J. KLINGENBERG, Simulated Strength of Wet Fibre Networks, JPPS 33(4) 2007 198-205

II. PASI P.J. MIETTINEN, JUKKA A. KETOJA, AND TUOMO HJELT, Simulated structure of wet fiber networks, NPPRJ 22(4) 2007 516-522

III. PASI P.J. MIETTINEN, AND JUKKA A. KETOJA, Simulation of triaxial deformation of wet fiber networks, NPPRJ 23(3) 2008 264-271

IV. PASI P.J. MIETTINEN, PASI KEKKO, JARMO KOUKO, Relaxation of wet paper by simulations and laboratory-scale experiments, accepted for publication in NPPRJ

The author of this thesis has performed all the simulations and almost all the analysis reported in this thesis. The author has written the first draft of articles I, II and III and parts of article IV. The author also actively participated in finalizing all these articles.

Contents

Chapter 1

1 Introduction

One of the most interesting research topics in material science is to understand how macroscopic properties of solids depend on the properties of their constituents and interactions between them. In fully ordered materials the structure is well defined and physical quantities are understood, but in disordered systems the situation is different depending on the degree of disorder. In several industrial applications controlling the magnitude of disorder is essential. An excellent example is the papermaking process which determines the structure and mechanical properties of paper.

The rheology of wet paper webs is technologically very important but poorly understood. In the papermaking process, the wet paper web is transported ("drawn") from the wire section through the press section and then to the dryer section. The purpose of these unit processes is to remove water from the web. Early in the process where the water content is large, the mechanical strength of the web is small. The low strength is one of the factors that limit the production speed of the paper machine. Reinforcement pulp is often needed to assure sufficient strength of the wet web. The use of reinforcement pulp increases raw material costs and the use of wood raw material in the papermaking process.

The mechanical and rheological properties of wet webs are surprisingly poorly understood despite their high relevance. Some experimental studies have been reported, but research has been limited in part by the lack of a suitable theoretical framework that could be used to interpret experimental results (Lyne and Gallay 1954a-1954c, Jantunen 1985 and Kurki et al. 2004). The mechanical rigidity or cohesion of the wet web can be attributed to water menisci that pull fibers into contact. Macroscopic deformations take place when fibers slide past one another. These deformations are strongly rate-dependent. It is unclear how rate-dependent phenomena should be incorporated into existing mean-field models, where the response of the network is expressed in terms of a single "average" fiber (Page 1993, Seth 1995 and Shallhorn 2002).

Recent development of computers has enabled one to probe the structure and mechanical properties of three-dimensional fiber networks also by simulations (Heyden 2000; Schmid et al. 2000; Switzer 2002; Switzer and Klingenberg 2003; Switzer et al. 2004; Lindström 2008). Switzer et al. (2002 and 2004) employed fiber level simulations to investigate the relationships between fiber properties (length, shape and flexibility) and interactions (friction) and the mechanical properties of wet webs. This study illustrated that it is not necessary to employ a mean-field approach to investigate wet webs, and that rate-dependent phenomena can be addressed in a straightforward manner via simulations. However, the authors did not consider the attractive force between fibers in wet webs generated by surface tension (Campbell forces (Campbell 1959)), and employed coefficients of friction that were admittedly unrealistically large.

In this Thesis, we extend the simulation method employed by Switzer et al. to investigate the mechanical and structural properties of wet webs. In Chapter 3 the computer simulation model and methods used are reviewed, but they are covered only briefly since they are described in more detail in publications and elsewhere (I, II, Schmid et al. 2000; Switzer 2002; Switzer et al. 2004). In particular, we include an attractive force between fibers in contact to represent the Campbell (surface tension) forces. We confirm that tensile strength of wet fiber networks can be expressed as a simple function of the adhesion force, number of inter-fiber contacts, coefficient of friction, and network grammage. The observed behavior is interpreted in terms of changes in the network structure during deformation.

Several authors (Corte and Kallmes 1962; Komori and Makishima 1977; Dodson and Deng 1994; Mäkinen 2001; Sampson 2001; He et al. 2003) have tried to see how far one can get with analytic structural models without considering the details of the forming process. The first successful structural models were presented already by Corte and Kallmes (1962) and by Komori and Makishima (1977). Their models were based on statistical analysis predicting the number of fiber crossings in a given volume for straight and rigid fibers.

We also use the simulation model of Switzer et al. (2004) for pressing and stretching a three-dimensional fiber network. The prediction of the number of inter-fiber contacts is of utmost importance, and it will be one of the main goals in this Thesis. We monitor the number of inter-fiber contacts during pressing and stretching and compare the simulation results to various analytic models. In addition, the fiber orientation and fiber curvature are evaluated during the simulation. It turns out that our simulations are most useful for flocculated and stretched sheets, where the simplifications of analytical model are not valid any longer. The orientation change due to stretching turns out to be too small to explain the deviation between analytic and simulation results. Instead, we find significant changes in the effective sheet area during stretching that affect the number of inter-fiber contacts.

When paper is strained in one direction, it deforms in perpendicular directions as well. This behavior is known as the Poisson effect (Stenberg and Fellers 2002). Göttsching and Baumgarten (1976) studied extensively triaxial deformation of *dry* paper under in-plane tensile load. Their experimental results show that the in-plane Poisson's ratio does not depend on the applied strain and Poisson's ratio in the thickness direction depends on the beating level. Seth and Page (1983), Habeger (1985) and Ramasubramanian and Perkins (1988) used micromechanical models to study the nonlinear behavior of fiber networks under tensile load. An excellent review of the topic can be found in the work of Heyden (2000), and Chapter 2 discusses the earlier work in the field of fiber network modeling. Chapter 2 covers mainly modeling efforts of *dry* networks when mean-field models are valid. For *wet* networks this approach cannot work since fibers are almost infinitely rigid compared to bonds. This means that fibers do not behave as fiber network on average.

In this Thesis, we also apply simulation methods to deformation of *wet* fiber networks in the lateral and in the thickness directions during straining. Another main focus is to determine triaxial deformations when the network is stretched beyond the elastic region. Such deformations are of interest for several practical reasons. First, changes in network thickness during stretching affect network porosity and thus the quality of

paper. On the other hand, the lateral network contraction alters the stress field of a wet web and thus contributes to the runnability of a paper machine.

According to our simulations, the lateral Poisson's ratio depends not only on the applied strain but also on the length of the specimen. The resulting stress fields may be similar to those in short-span tensile tests. The gap length affects the simulated stress-strain curves qualitatively in the same way as seen in the experiments by Batchelor and Westerlind (2003). Moreover, the network deformations turn out to be sensitive to fiber stiffness. Usually the network thickness decreases during stretching but for very stiff fibers, the network slightly expands in the thickness direction as proposed by earlier experiments for wet papers (Baum et al. 1984). In addition to deformations, we revisit the theory of tensile strength for wet paper webs. The validity of our failure criterion is studied for varied network geometry and sample size.

Rate-dependent viscous behavior such as stress relaxation and creep characterizes the rheological behavior of paper (Niskanen 1998). Already in the 1950's and the 1960's several authors showed that the strength of wet webs starts to develop at very low solids contents. Lyne and Gallay (1954a-1954c), Page and Tydeman (1965) and Robertson (1963) illustrated experimentally the importance of surface tension forces and interfiber bonding to the strength development of wet sheets. Lyne and Gallay (1954a) measured wet web strengths at solids contents as low as 8 %. They defined an infliction point at solids content of 20-25 % where interfiber bonding replaces surface tension forces as a major factor contributing to the wet strength. They were also among the first to measure rheological properties of wet webs, namely loading and de-loading curves for solids contents below 20 % (1954c). Page and Tydeman (1965) and Robertson showed that interfiber bonding occurs at solids contents of 45-50 %. Page and Tydeman provided sets of visual evidence and Robertson investigated extensively physical properties of wet webs as water was progressively removed.

Drying paper under load while preventing shrinkage has a great effect on the mechanical properties of paper, e.g. elastic modulus, strain, tensile strength and dimensional stability (Htun and de Ruvo 1977, Salmén et al. 1987). Similar effects are also reported with single fibers (Kallmes and Perez 1965, Duncker et al. 1965).

In stress relaxation experiments, a paper sample is strained to a predefined strain. There after the strain is kept constant, and stress decreases as a function of time. Stress relaxation is of great importance in a wound paper roll, or when handling deformable paper webs (Makela 2007), e.g., in the open draws of a paper machine dryer section or in a printing machine (Niskanen 1998). In a wet (high moisture content) paper web tension relaxes rapidly and gives rise to a permanent elongation (Niskanen 1998).

It was already shown by Craven (1962) that stress relaxes logarithmically in time,

$$\sigma(t) = const - R\log(t). \tag{1.1}$$

Here R is the relaxation rate which was shown by Johanson and Kubat (1964) to be related to difference of the initial (σ_0) and equilibrium (σ_∞, i.e., its asymptotic value in a relaxation experiment) stresses,

$$R = k(\sigma_0 - \sigma_\infty) \tag{1.2}$$

with k a constant. Only very few studies can be found in the literature on stress relaxation in wet paper. After the work by Lyne and Gallay (1954c), Jantunen (1985) used laboratory-scale equipment to simulate dynamic behavior of wet webs. He investigated stress relaxation at various solids contents and prescribed strains, and showed that tensile force relaxes faster in wet than dry paper, and that increasing applied strain systematically increases the relaxation speed in wet paper. Very recently Kouko et al. (2007) performed stress-relaxation experiments on wet paper at varying strain rate and short relaxation times, and tried to link results of laboratory-scale experiments to paper-machine runnability. In another recent work Makela (2007) developed an accurate method for characterization of viscous properties of paper. Effects of straining level, moisture ratio and restrained drying on the stress relaxation of paper were determined. A stress-relaxation modulus (tensile force scaled by the elastic strain) was used to compare the behaviors of paper samples of varying moisture ratio and drying restraint. The investigated paper samples were concluded to display linear viscoelasticity.

Relaxation processes in a wet paper web can also be simulated numerically. We report here simulated relaxation results for random networks of non-bonded fibers, and compare them with those of laboratory-scale relaxation experiments on wet paper. In addition, we observe breaks of fiber-fiber contacts in these simulations.

In Chapter 4 we present our simulation results for the mechanical properties of wet webs. Comparison with experiments on tensile strength and tensile-force relaxation are shown. We then discuss the simulated structure and deformations of wet fiber networks, and compare these results with analytical solutions and earlier experiments. Finally, in Chapter 6, we draw conclusions and discuss the results of this thesis.

Chapter 2

2 Earlier work on fiber-network modeling

The classical paper by Cox (1952) was the first to discuss the mechanical properties of fiber networks by theoretical analysis. In his model long, straight fibers carried only axial load with no interaction between them, and the fibers extended across the whole network (Fig. 1). The fibers of the network were oriented according to a distribution function. He assumed that fibers were bonded to some background medium, and that the strain field was homogeneous throughout the network. In the case of isotropic fiber orientation, the elastic modulus of the network is then given by

$$E_{\mathrm{mod}} = \frac{1}{3}\frac{\rho_s}{\rho_f} E_f \,. \tag{2.1}$$

Here E_f is the elastic modulus of the fiber, ρ_s the network density, and ρ_f the fiber density. The ratio of lateral network strain ε_y to the applied strain ε_{x} for isotropic orientation, namely the Poisson ratio, becomes $\nu_{xy} = 1/3$.

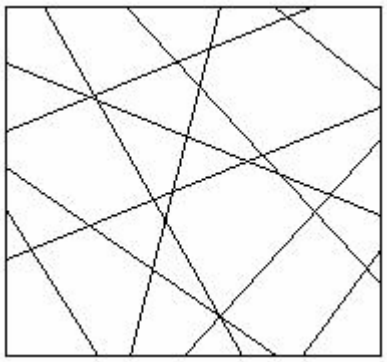

Figure 1. A Cox-model network

For dry sheets of long, straight and well-bonded fibers, experimental results support this finding for the elastic modulus of the network (Page et al. 1979; Page and Seth 1980). In reality, network modulus is smaller than Eq. (2.1) implies such that (Page et al. 1979; Page and Seth 1980)

$$E_{\mathrm{mod}} = \frac{1}{3}\frac{\rho_s}{\rho_f} E_f (1 - pE_f^{1/2}) \,. \tag{2.2}$$

Parameter p is a function of fiber geometry, shear force, and relative bonded area (*RBA*) due to limitations in load transfer between the fibers of finite length and defects in the fibers.

Later, Seth and Page (1983) and Habeger (1985) extended the analysis of Cox from the elastic to nonlinear region by assuming that the fibers were entirely responsible for the inelastic behavior of the network. Habeger (1985) showed that the lateral

Poisson ratio decreases with increasing applied strain when a network is strained beyond the elastic region.

In their work, Ramasubramanian and Perkins (1988) used a more complex micromechanical model and incorporated the inelastic behavior of fibers and bonds to describe the nonlinear behavior of fiber networks under tensile load. This micromechanical model includes three levels of magnification: a microelement consisting of a portion of two crossing fibers with an interfiber bond, a mesoelement consisting of a straight fiber and a portion of fibers that cross it, and a macroelement described by a large number of mesoelements with orientation and length distributions. On the macroelement level, they assumed a homogeneous strain field, and that fibers experience axial tensile or compressive loads.

Eventually, a closed-form expression for the work done on the mesoelement W_{MESO} is provided for specified strain ε_x with a set of possible lateral contraction ratios ν_{xy}, and then the total work done on the macroelement is calculated for each choice of lateral contraction ratio by numerical integration of

$$W_{TOTAL} = \int_0^{\infty} \int_{-\pi/2}^{\pi/2} D_o W_{MESO} f(\theta) g(L) d\theta dL . \tag{2.3}$$

Here D_o is the number of mesoelements per unit area, and $f(\theta)$ and $g(L)$ represent the orientation and fiber length distributions, respectively. The correct value of the lateral contraction ratio is obtained by requiring that the total work is minimized ($\partial W_{TOTAL} / \partial \nu_{xy} = 0$), and substituting it to the equation describing the sheet strain in the direction of the fiber,

$$\varepsilon_s = \varepsilon_x \left(\cos^2 \theta - \nu_{xy} \sin^2 \theta \right). \tag{2.4}$$

Finally, the stress-strain relation is obtained by

$$\sigma_x = \frac{\partial W_{TOTAL}}{\partial \varepsilon_x} . \tag{2.5}$$

In addition to work presented in Ramasubramanian and Perkins (1988), Ramasubramanian (1987) provides more detailed information of the micromechanical model and the computer simulation procedure discussed here. Their model contains interesting features found in wet webs such as low bonding with an elastic-plastic behavior and minimal fiber damage during loading. However, the power of these kinds of models is limited due to a large number of parameters needed, many of which are not possible to measure. In addition, the stochastic nature of fiber networks is ignored as noted by Niskanen (1998).

Recent development of computers has enabled one to probe the structure and mechanical properties of three-dimensional fiber networks also by simulations. Heyden (2000) was among the first to do so by modeling mechanical properties of cellulose fluff. She also used two-dimensional networks. In her model, a basic building block is an isotropic linearly elastic fiber, which is divided into beam

elements between bonds. The fiber is modeled as a Bernoulli beam of circle-arc shape (Fig. 2), and it is assumed to fail in a brittle manner.

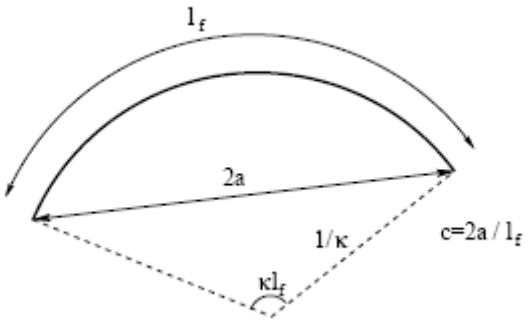

Figure 2. Definition of curl index *c* and curvature κ for a fiber of length l_f according to Heyden (2000). Figure taken from her Doctoral Thesis.

A fiber-fiber bond is modeled using either coupled or uncoupled springs which distribute normal and shear stresses between contacting fibers. The bonds show nonlinear stick-slip behavior, and when a slip criterion is fulfilled, the stiffness and strength of the bond are reduced by predefined factors. Finally, the three-dimensional structure of cellulose fibers is constructed by placing fibers independently of each other in a volume *V* (Fig. 3). The orientation of each fiber is decided according to a predefined orientation distribution. In addition, a fiber-fiber contact is assumed to occur with a probability of *s* when the distance between two fiber center lines is shorter than an arbitrary interaction distance, *e*.

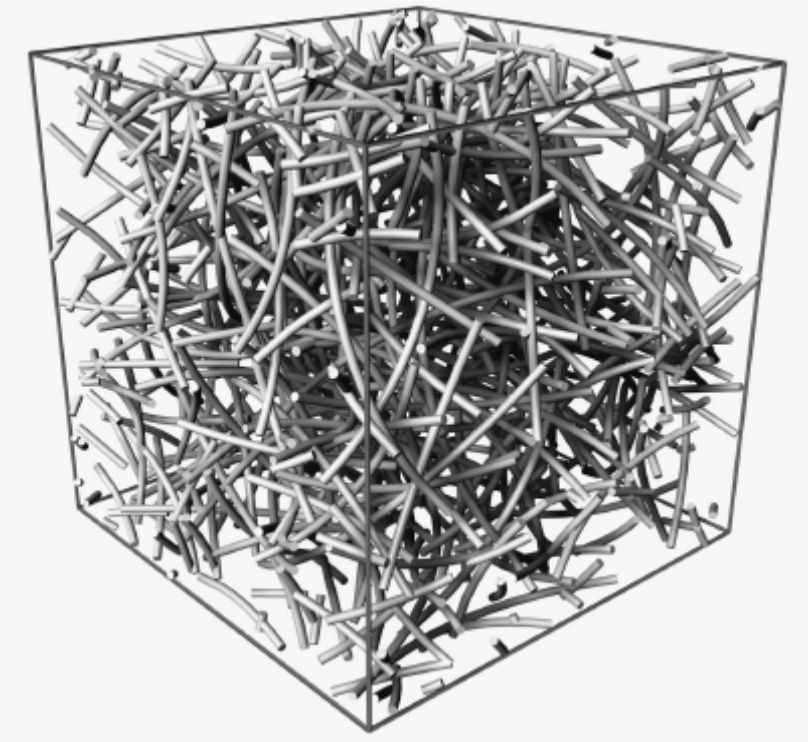

Figure 3. Example of 3D network geometry. Figure taken from the Doctoral Thesis of Heyden (2000).

Heyden used the finite-element method to obtain the stress-strain behavior of the network. Simulations showed effects of fiber and bond stiffness, network density, fiber curl, fiber orientation distribution and fiber length on the network stiffness. Fracture simulations showed the importance of bond ductility in 2D networks, increasing ductility resulting in a stronger and more ductile network. Based on these results, it seems that this model is suitable for studying the mechanical response of dry sheets as noted by Switzer et al. (2004). In addition, Heyden (2000) provides an excellent and detailed review of the earlier fiber network modeling.

Åström et al. (2000a) improved the Cox model by considering fiber segments as the basic building blocks since the stresses, in a fiber network, are transferred at the fiber-to-fiber crossings, and took into account the known segment-length distribution of randomly deposited fibers. They assumed that fiber segments deform only in the energetically most favorable modes (bending, stretching and shearing) depending on their orientation and length, and used the displacement field of the Cox model to eventually obtain the stiffness of a two-dimensional network. They compared this modified effective-medium model with simulation results and experimental findings, and found fairly good agreement between simulations and the model, and that the stiffness of the modified network model was consistent with experiments.

Åström et al. (2000b) investigated the in-plane stiffness of fiber mats by analytical and numerical models. They extended the two-dimensional simulation model and the effective-medium model of the in-plane stiffness of 2D mats (Åström et al. 2000a) to three-dimensional fiber networks. In 3D, linear elastic fibers with a cross-sectional area w^2 were deposited vertically on a plane at random positions with random in-plane angles. Fibers were bent at contact points by a bending angle ϕ. Finally, the fiber network was formed by linear segments between different types of nodes, and at contact nodes (crossings of fibers) two fibers were rigidly bonded. Then the resulting network was strained, and its stiffness was determined.

For small bending angles (ϕ = 0.01-0.05), the simulated stiffness of the 3D mat was equal to the simulated stiffness of its 2D projection for various network densities q and fiber widths w. In addition, the 3D analytical estimation obtained for in-plane stiffness captured extremely well the simulated result for small bending angles (ϕ = 0.03-0.11). For large bending angles ($\phi > 0.1$), the analytical prediction of the in-plane stiffness initially increased with increasing bending angle due to better bonding, but started to decrease when a large enough out-of-plane deformation was reached. This behavior was related to the fact that the bending stiffness of fibers was clearly lower than their axial stiffness, since the in-plane fibers resist most the in-plane stretching.

Later, Åström et al. (2003) showed that the effective-medium estimate for mats of randomly sedimented elastic fibers connects the network stiffness to the fiber stiffness and the fiber geometry, and to the number density of contacts. They demonstrated that the number density of contacts and the fiber geometry also determine the network porosity. More recently, Lindström (2008) developed a particle-level model of fiber suspension flows for the forming section of the paper machine. His model included fibers of various shapes and finite stiffness. The model fibers interacted via normal, frictional and lubrication forces, and a two-way coupling between the fibers and a surrounding fluid medium was taken into account. His simulations captured essential features of the forming effects on structural parameters of paper.

Chapter 3

3 Simulation method

The computer simulation model and the methods used in this Thesis are described in more detail in publications (I, II) and elsewhere (Schmid et al. 2000; Switzer 2002; Switzer et al. 2004). Here we will thus present only the basics and essential features of the model.

Flexible fibers are modeled as joined rigid cylinders with hemispherical end-caps immersed in a Newtonian liquid as illustrated in Fig. 4. The fiber length is $L = 2lN_{\mathrm{seg}}$, where N_{seg} is the number of fiber segments and $2l$ is the segment length. Isolated fibers are not typically straight at equilibrium, but can display a variety of different shapes. Equilibrium angles $\left(\theta^{eq}, \phi^{eq}\right)$ between the axial directions of successive cylinders were used to characterize the fiber shape. When both angles are zero, the fiber is perfectly straight, and when $\theta^{eq} > 0, \phi^{eq} = 0$ the fiber is U-shaped. When both angles are nonzero, the fiber is a helix. The equilibrium angles used in most of our simulations were $\theta^{eq} = 0.1, \phi^{eq} = 0.0$ corresponding to nearly straight fibers.

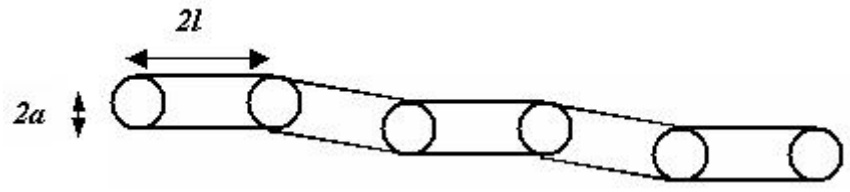

Figure 4. A model fiber composed of N_{seg} = 5 rigid segments. The segment length is $2l$ and the fiber diameter is $2a$.

Particle and fluid inertia are neglected. The fluid is needed to make equations easily solvable. Otherwise, the role of the fluid remains small. The motion of each fiber segment is governed by Newton's equations of motion,

$$\vec{F}_i^h + \vec{X}_{i+1} - \vec{X}_i + \sum_j \vec{F}_{ij} = 0\,, \tag{3.1}$$

$$\vec{T}_i^h + \vec{Y}_{i+1} - \vec{Y}_i + l\vec{p}_i \times \left(\vec{X}_{i+1} + \vec{X}_i\right) + \sum_j \vec{T}_{ij} = 0\,. \tag{3.2}$$

In the first equation, $\vec{F}_i^h$ is the hydrodynamic drag of the segment, $\vec{X}_i$'s are the forces at the joints at the two ends of segments, which keep its length constant, and $\sum_j \vec{F}_{ij}$ represents the forces caused by interaction of the segment with other fibers. In the second equation, $\vec{T}_i^h$ is the hydrodynamic torque of the segment, $\vec{Y}_i$'s are the sums of the bending and twisting torques, $\vec{Y}_i^b$ and $\vec{Y}_i^t$, at the joints, $\vec{p}_i$ is the orientation vector of the segment, and $\sum_j \vec{T}_{ij}$ describes the torque introduced by interaction with other fibers. Moreover,

$$\left|\vec{Y}_i^b\right| = k_b\left|\theta_i - \theta_i^{eq}\right| \ , \ \left|\vec{Y}_i^t\right| = k_t\left|\phi_i - \phi_i^{eq}\right|, \tag{3.3}$$

where k_b and k_t are the bending and twisting spring constants, and θ and ϕ the bending and twisting angles of the segment, respectively.

Interaction forces between fibers are divided into two components, $\vec{F}_{ij} = F_{ij}^N \hat{e}_N + F_{ij}^\perp \hat{e}_\perp$. The normal force F_{ij}^N depends on the separation h between the surfaces of fibers i and j, and includes a short-range repulsive interaction (to prevent fibers from overlapping) and a longer-range attractive interaction. This force is modeled as $F_{ij}^N = -\mathrm{Re}^{-c_1(h/a)} + Ae^{-c_2(h/a)^2}$, where R, c_1, c_2 and A are parameters that characterize the magnitude and range of the normal force. The parameters $c_1 = 20$ and $c_2 = 35$ were kept constant in the simulations, and the parameters R and A were varied simultaneously so that a minimum in $F_{ij}^N(h)$ was reached at equal separation h for all adhesion forces. In fact, we define the adhesion force $F_{ad}(>0)$ as the absolute value of the minimum in $F_{ij}^N(h)$ as illustrated in Fig. 5. The adhesion force models the Campbell force caused by water bridges between fiber surfaces.

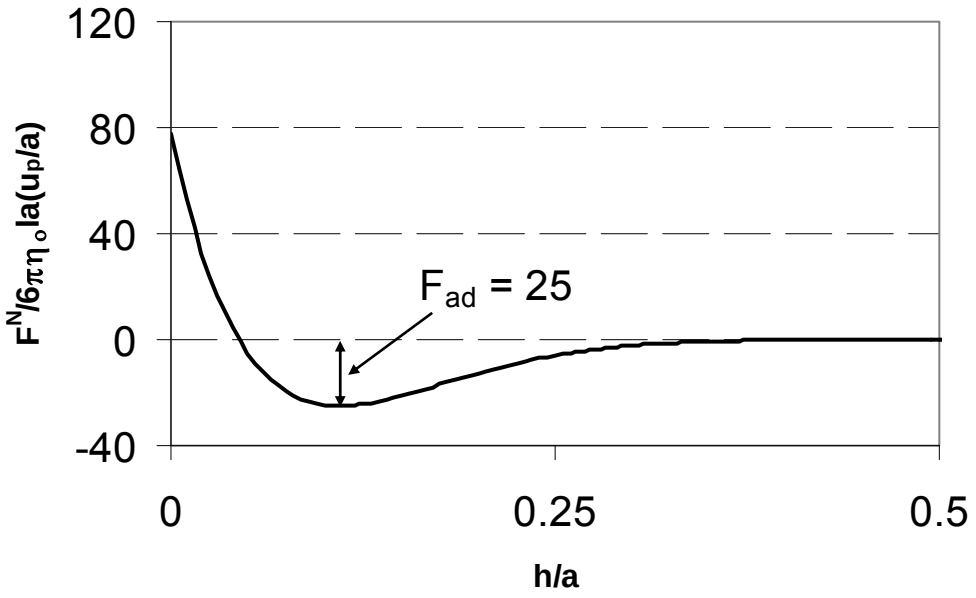

Figure 5. Dimensionless normal force as a function of dimensionless surface separation *h/a*. F_{ad} is the adhesion force between surfaces (maximum attraction). The scaling parameters of the force are explained in the next section.

The other component, $F_{ij}^\perp$ points along the fiber surface at the points of contact, and it is this component (or rather the motion induced by it) which is affected by friction. The friction between fibers in contact is simulated by requiring that there is no relative (tangential) motion at contact points unless the absolute value of the affecting force, $\left|F_{ij}^\perp\right|$, exceeds the static friction limit, $\mu\left|F_{ij}^N\right|$ with μ the static friction coefficient. If $\left|F_{ij}^\perp\right| > \mu\left|F_{ij}^N\right|$ at one or more contact points, the largest value of $\left|F_{ij}^\perp\right|$ is removed,

and the tangential forces are recomputated. This procedure is repeated until $\left|F_{ij}^{\perp}\right| \le \mu \left|F_{ij}^{N}\right|$ at all contact points (Schmid 1999). At the contact points where $\left|F_{ij}^{\perp}\right|$ was removed, the fibers in contact are allowed to slide unimpeded except for the hydrodynamic drag (approximated as that for an isolated prolate spheroid). In the simulations the friction coefficient is $\mu = 0.5$.

The fiber network, whose behavior under tensile loading was to be tested, was formed by a two-step process. First, an initial network was constructed by placing fibers randomly in a 3D simulation box with uniform center-of-mass distribution and fiber orientation (Fig. 6a). The typical simulation box has the length $2L$ in all directions. Thereafter this 3D structure was compressed into a planar structure that modeled paper. This compression was realized using a plate on top of the simulation box. This plate was let to fall in the negative z direction due to gravity. The bottom plate of the box was permeable only to the fluid. Periodic boundary conditions were used in the x and y directions. The fiber network was thus compressed into the desired planar shape with a plate spacing of $20a$. (Figs. 6b and 6c).

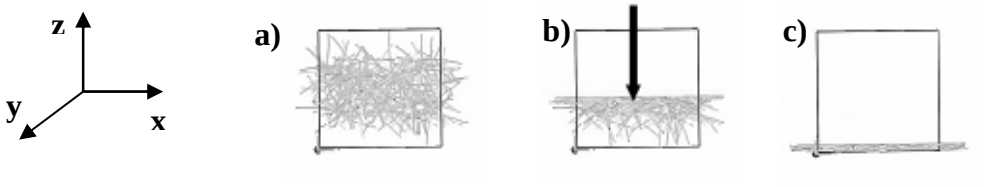

Figure 6. a) Randomly generated structure of fibers b) compression the generated structure, and c) the resulting planar network that will be subjected to tensile loading.

Once the desired planar structure is reached, the network is relaxed by integrating the equations of motion for fiber segments until all motion ceases. During relaxation the attractive forces are applied between fibers and the fiber motion slows down exponentially. Relaxation was taken to be completed when the mean square fiber-segment velocity decreased below a predetermined threshold ($0.001\,u_p^2$). Friction was ignored during compression and relaxation, but was enforced during tensile testing.

Tensile testing of the fiber network was modeled by pulling at the fiber segments that intersected the faces at $x = \pm L_x/2$ of the simulation box at a constant velocity $\pm u_p$ (as illustrated in Fig. 7). Figure 8 shows a fiber network used in tensile testing. The force applied to pulling the crossing fibers at the left and right ends of the simulation box also indicated in Fig. 8, $\vec{F}_i^{\,p}$, is added to Eq. (3.1) and is treated as a constraint evaluated at each time step during the simulation. The corresponding torque $d_i \vec{p}_i \times \vec{F}_i^{\,p}$ is added to Eq. (3.2). Here d_i is the distance from the segment center to the location of the externally applied force. Once each force $\vec{F}_i^{\,p}$ is known, the tensile force is determined as

$$\vec{T} = \frac{1}{2}\left(\sum\nolimits_{rface} \vec{F}_i^{\,p} - \sum\nolimits_{lface} \vec{F}_j^{\,p}\right), \tag{3.4}$$

where r_{face} and l_{face} refer to fiber segments that cross the simulation box at the face x = + $L_x/2$ and x = - $L_x/2$, respectively.

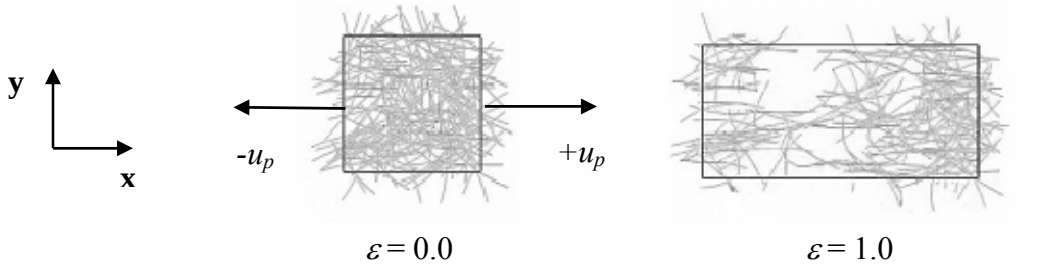

Figure 7. Typical fiber network before and after tensile testing. Strain is relative change in sample length $\varepsilon = 2\Delta x/L_x$.

In order to reduce the number of parameters, we defined the following dimensionless forces and torques:

$$F_i^{N*} = \frac{F_i^N}{6\pi\eta_o la\dot{\gamma}}, \quad F_i^{fric*} = \frac{F_i^{fric}}{6\pi\eta_o la\dot{\gamma}}, \quad X_i^* = \frac{X_i}{6\pi\eta_o la\dot{\gamma}}, \; Y_i^* = \frac{Y_i}{8\pi\eta_o l^3\dot{\gamma}}, \tag{3.5}$$

where η_o is the viscosity of the background fluid, $2l$ is the segment length, a is the fiber radius and $\dot{\gamma} = u_p / a$. A dimensionless bending constant k_b^* arises naturally from Eqs. (3.3) and (3.5),

$$k_b^* = \frac{k_b}{8\pi\eta_o l^3\dot{\gamma}}. \tag{3.6}$$

The twisting constant is assumed to be directly proportional to the bending constant, $k_t^* / k_b^* = 0.67$, which is equivalent to that of an elastic cylinder with a Poisson's ratio of 0.5. In the following chapters, only dimensionless quantities are used, and the superscripted asterisks are omitted.

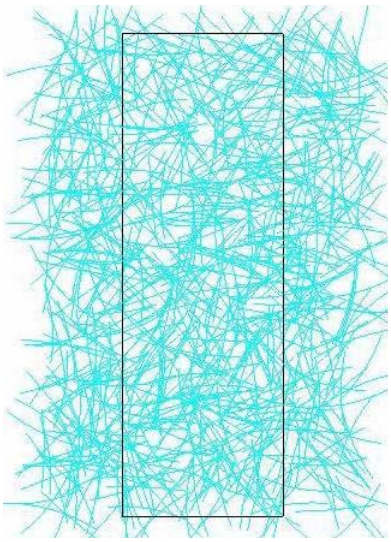

Figure 8. An equilibrium fiber network ready for tensile or relaxation testing. The black lines indicate the borders of the simulation box.

Chapter 4

4 Mechanical properties of wet fiber networks

In this chapter we consider simulation results for stress-strain curves, tensile strength and relaxation of wet webs. Publications I and IV discuss these results in more detail.

4.1 Stress-strain curve

When a strip of paper or a fiber network is subjected to an external strain ε, a force response is recorded. Typical force-strain curves (at constant straining velocity) from simulations are presented in Fig. 9 (upper panel) Three strain recovery curves are also shown in this figure, i.e. the behavior of strain when the tensile force was brought back to zero at three different strain levels (ε_x = 0.9 %, 5.0 %, and 9.0 %). In the figure the tensile force is scaled by the network grammage b, the number of contacts per fiber N_c, and the ratio of sample width to fiber length, L_y/L. Most of the deformation caused by straining is plastic, as strain recovery is quite small. For comparison we show in the lower panel of Fig. 9 two similar force-strain curves from laboratory scale experiments on wet paper in which samples were strained at a constant strain rate of 5.6 %/s to ε_x = 0.9% and 3.5% strain Thereafter the samples were kept fixed for 6 seconds, and de-strained at constant velocity until the tensile force reached zero. In the figure, the measured tensile force at 3.5% strain was scaled to unity.

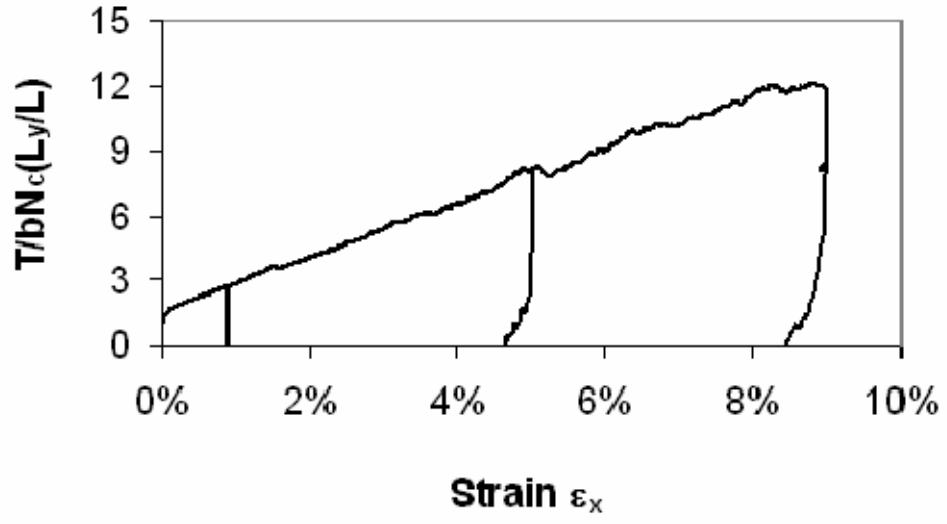

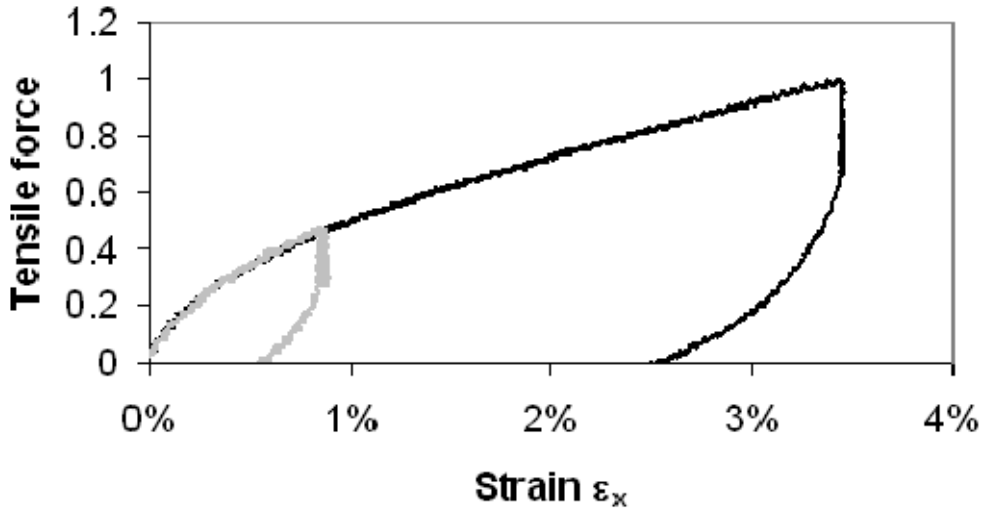

Figure 9. Scaled tensile force as a function of strain from simulations (upper panel, average of five independent runs) and experiments (lower panel). Experimental data are for fine paper with a grammage of 60 g/m^2 and a solids content of 60%.

It is evident from Fig. 9 that qualitatively the simulated and measured force-strain behaviors are very similar. The main difference is the much larger strain recovery in real wet paper. With the scaling used above for the simulated tensile force, fluctuations in this force do not appreciably show up. We show therefore in Fig. 10 the result of another tensile straining simulation for a single network in which the force is scaled as shown in Eq. (3.5). Otherwise the forces in Figs. 9 and 10 are scaled in a similar manner. Force fluctuations are now apparent. They are caused by fiber contacts breaking and reforming as found experimentally by Switzer et al. (2004). At large strains when the network is broken into two separate parts, the tensile force is small but nonzero because of the hydrodynamic drag forces exerted on fibers. Because of the small size of the simulation box in comparison with paper samples typically used in experiments, force fluctuations are much more pronounced than in experiments on paper. Notice also that in the result of Fig. 10 tensile straining is continued beyond the breaking point.

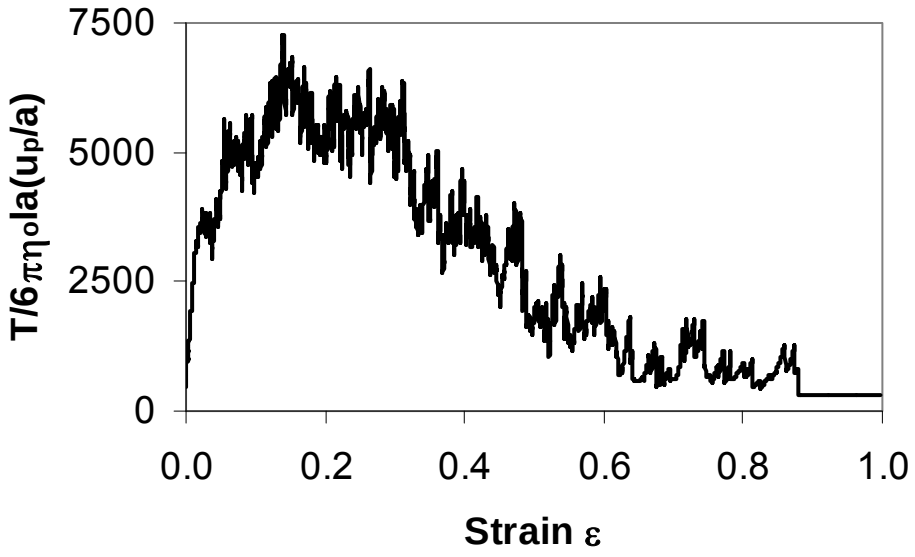

Figure 10. Dimensionless tensile force as a function of strain. Adhesion force was F_{ad} = 250 and fiber stiffness k_b = 75.

4.2 Tensile strength

In Fig. 11, the tensile strength obtained by simulations is plotted as a function of $\mu b N_c F_{ad} / \omega$. Here μ is the friction coefficient between fibers (μ = 0.5 in the simulations), b is the network grammage (a mass of the fiber network per area), N_c is the number of contacts per fiber at maximum tensile force (tensile strength), F_{ad} is the adhesion force and ω is the fiber coarseness (a fiber mass per fiber length). The different symbols represent simulations for a variety of fiber stiffnesses, shapes, lengths, adhesion forces and sheet densities, yet the data fall onto a single curve. We note that although the fiber shape, aspect ratio, and stiffness do not appear explicitly in the equations, they do influence such parameters as b, N_c and ω.

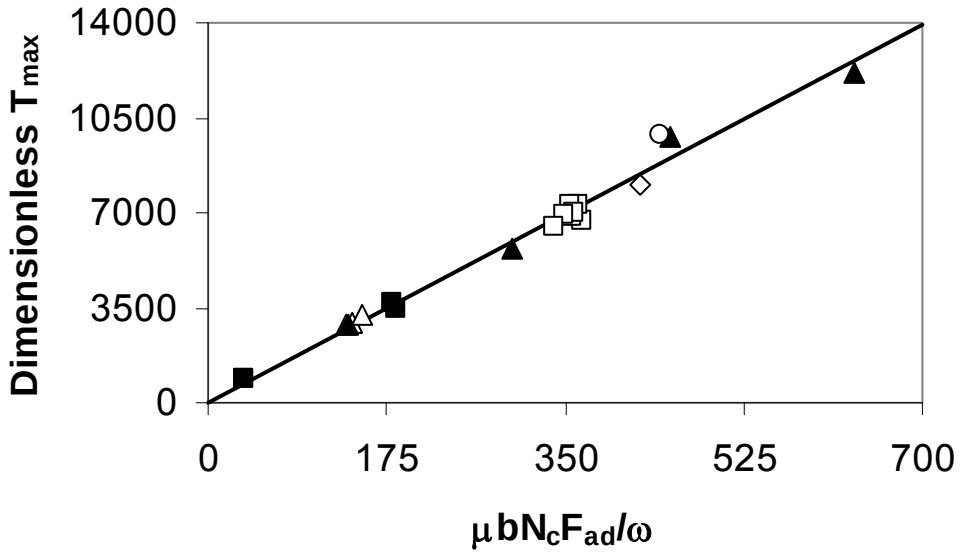

Figure 11. Dimensionless tensile strength of simulated fiber networks as a function of □ varying fiber stiffness, ■ varying adhesion force, ▲ varying adhesion force with low network grammage, △ varying fiber shape, and varying fiber aspect ratio: 50 (□),70 (◊) and 90 (○).

Our simulations show that that the strength of wet fiber networks depends only on a single variable composed of a few network and fiber properties very much as suggested by Page (1993), such that

$$T_{\max} = \mu b N_c F_{ad} / \omega . \tag{4.1}$$

4.3 Relaxation of wet paper

When tension is applied on a sheet of paper or a fiber network so that it is held at constant length its tension decreases with time (Craven 1962). This phenomenon is called stress relaxation. Stress relaxation results are shown in Fig. 12 for simulations as well as experiments. Simulated tensile force relaxation compares well with the experimentally observed relaxation for wet sheets of paper: in both cases tensile force decreases under relaxation rather linearly with logarithmic time.

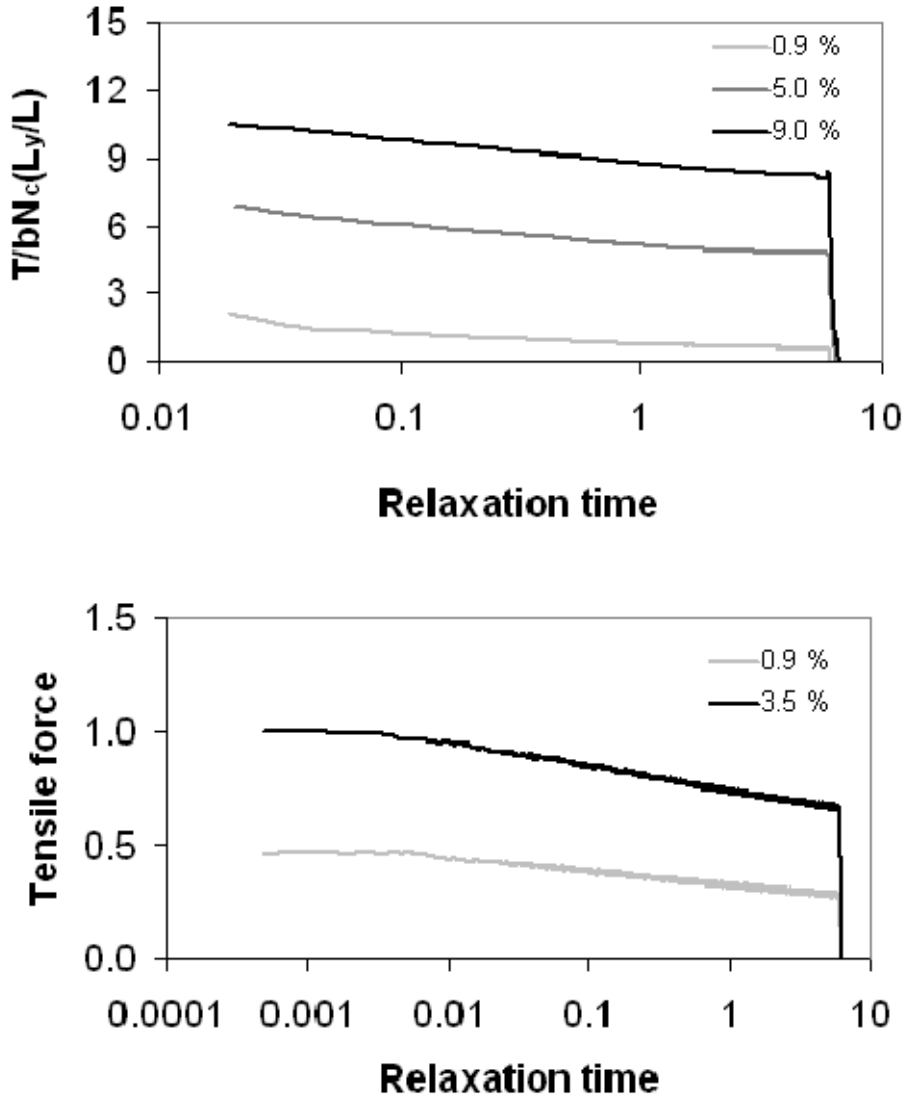

Figure 12. Tensile force relaxation for simulations (three curves in the upper panel, strain increases from bottom to top) and experiments on wet paper (two curves, strain increases from bottom to top).

As noticed above, strain recovery in simulations was clearly smaller than in experiments on real paper. In order to quantify this effect, we compared the simulated and measured strain recovery during relaxation. The results of this comparison are shown in Fig. 13. The experimental strain recovery is about four times bigger than the simulated one. There are a few possible reasons for this difference. Complete lack of bonding in the simulated networks is one possible reason, and the description used for the interaction between wet (non-bonded) fibers is another possibility. A more detailed analysis of this effect is however beyond the scope of this study.

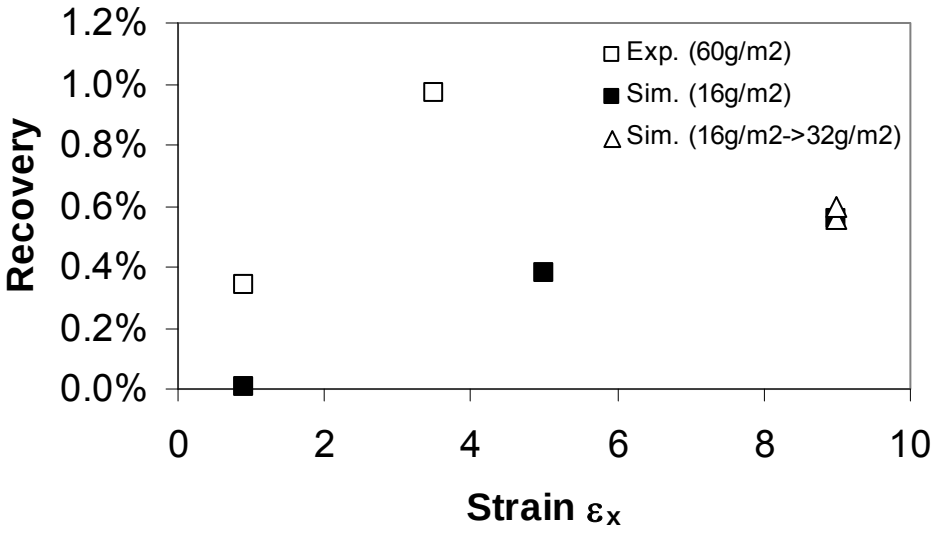

Figure 13. Comparison of experimental and simulated strain recovery after relaxation at varying strain.

Chapter 5

5 Structure and deformations of wet fiber networks

In this Chapter simulation results for the structure and deformations of wet fiber networks are shown for equilibrium structures and during mechanical testing. We present results and estimates for the sheet thickness and number of contacts per fiber together with estimates for strain in the lateral and thickness direction during a tensile test. In addition, the effect of fiber stiffness on sheet thickness is described. Publications II and III discuss these results in more detail.

5.1 Simulated structure

For an isotropic and thin fiber network (network thickness h is not much larger than the fiber diameter d), the number of contacts per fiber can be estimated by (Corte and Kallmes 1962)

$$N_c^{thin} = \frac{2dN_f L^2(2h-3d)}{\pi A(h-d)^2}. \tag{5.1}$$

Here N_f is the number of fibers in the network area A, and L is the fiber length. Equation (5.1) is derived using 2D network statistics in the case when 2D layers are stacked above one another.

Our simulated networks can be regarded as thin structures, and we define the simulated sheet thickness h to be the thickness that includes 80 % of the fibers. This estimate mimics an experimental thickness measurement on paper, where paper is pressed between two plates. The threshold value 80 % is obtained from experiments. Figure 14 shows a typical fiber network structure after compression and relaxation. The box illustrates the thickness determination.

Figure 14. A side view of a fiber network for the adhesion force F_{ad} = 250 and the fiber stiffness k_b = 50. The sheet thickness h is defined by the box that includes 80% of the fibers.

In Fig. 15 we show a simulated number of fiber contacts in equilibrium as a function of plate gap Z_{top}, and compare it to the analytical estimate Eq. (5.1). The plate gap is defined as the distance between the top and bottom plates during compression. They are removed before the relaxation phase. For large plate gaps (large network thicknesses), simulated structures have more inter-fiber contacts than the theoretical estimate, since randomly oriented fibers have more contacts in 3D than in the xy plane. For plate gaps in the range $0.2L$ – $0.6L$ = 20-60**,** the simulated number of inter-fiber contacts is quite close to the estimate. Apparently, a majority of the fibers close to the top plate lie roughly in the xy plane. Moreover, the estimation method for sheet

thickness successfully excludes the fibers close to the bottom plate, whose orientations deviate significantly from the xy plane.

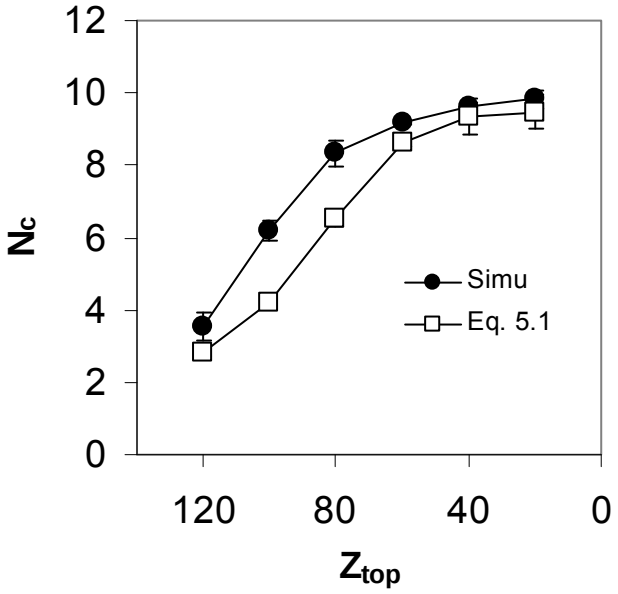

Figure 15. Comparison of the number of contacts per fiber N_c as obtained from simulations and from the theoretical estimate (Eq. (5.1)) as a function of plate gap Z_{top}. At Z_{top} = 20 = 0.2L = 10d compression is stopped, and the fiber network is ready for a tensile test. The results shown are averages over three random configurations, and the error bars indicate the standard deviation. The number of fibers is N_f = 256, the adhesion force is F_{ad} = 25, and the fiber stiffness is k_b = 50.

In Fig. 16 we show the number of contacts in equilibrium for wet fiber networks with varying fiber stiffness (k_b = 50 – 5000), adhesion force (F_{ad} = 25 - 1000), and network grammage (N_f = 64 - 256 corresponding to 8 - 32 g/m^2 for normal fiber properties). This figure compares the estimated number of fiber contacts (Eq. (5.1)) to that of the simulations. Agreement between the analytical estimate and the simulations is quite good for both the lowest (N_f = 64, $h \approx 4d$) and highest grammage (N_f = 256). For intermediate grammages, the analytical expression slightly underestimates the number of fiber contacts, but the overall correlation is good. In our basic network simulations (N_f = 128), we varied also the fiber length L**.** The relatively low values of the analytical estimate for all L is perhaps a result of the fact that we used only one initial network. For low grammage, the simulated number of inter-fiber contacts is slightly smaller than the analytical prediction. This might be due to the number of fibers being too small or to the network thickness being underestimated. Anyway, these results indicate the importance of the three-dimensional nature of the network.

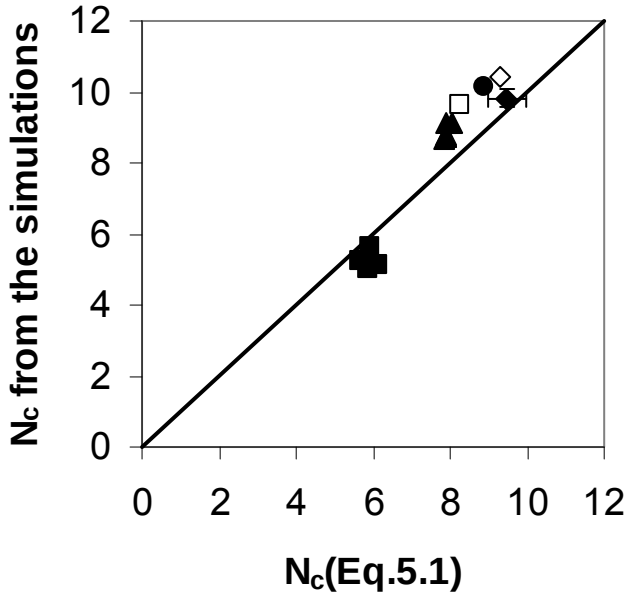

Figure 16. Comparison of the simulated and analytically estimated (Eq. (5.1)) numbers of contacts per fiber. Symbols are: (■) number of fibers N_f = 64 with varying adhesion force, (▲) number of fibers N_f = 128 with varying adhesion force and fiber stiffness, (□) number of fibers N_f = 192, (♦) number of fibers N_f = 256 (3 runs), fiber length L (aspect ratio r_p) (▲) 50, (●) 70 and (◊) 90.

Figure 17 shows the simulated number of inter-fiber contacts for stretched networks with varying fiber stiffness and adhesion force. For the basic network, the simulated number of fiber contacts is 15 – 20 % larger than the analytical estimate (Eq. 5.1), when the stretched area is used for A. The discrepancy between simulated and analytic values gets bigger for decreasing grammage: the simulated number of fiber contacts is clearly underestimated (by 35-60 %) by the analytical estimate. Moreover, during stretching the simulated N_c increased unexpectedly. There is at least one possible reason for the observed behavior. Figure 18 shows the web structure when the maximum tensile force is reached. The fibers do not spread out uniformly. Instead, they form flocs that contribute significantly to the number of contacts per fiber, and thus violate the validity of Eq. (5.1).

The above fiber clustering due to stretching can be analyzed in more detail by determining an effective sheet area A_{eff} occupied by fibers for both an unloaded and a deformed network at the maximal force. We define the effective sheet area as the part of the network where all pore areas are smaller than l_s^2 , where $l_s = \pi A/2N_fL = 2\pi L/N_f$ is the average distance between fiber crossings for a random two-dimensional isotropic fiber network (Komori and Makishima 1977). When comparing the effective areas of the unloaded and deformed networks, we find $A_{eff}^{\max} / A_{eff} = 0.83$ for the network of Fig. 18. In particular, the effective area for the deformed network after stretching is only 17% of the total area.

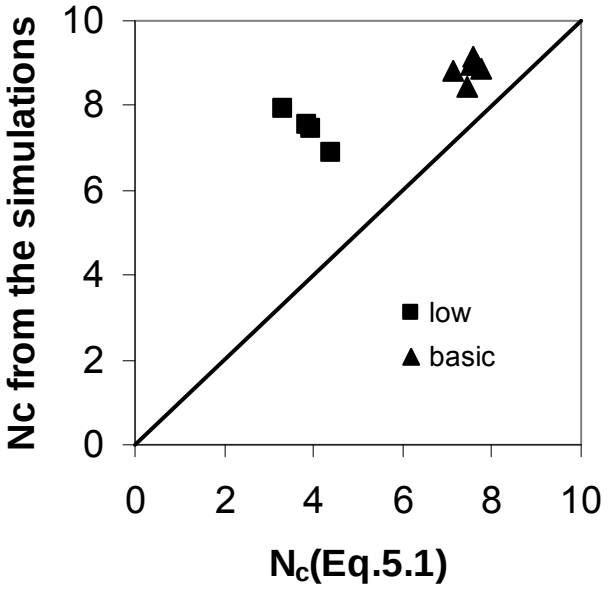

Figure 17. Comparison of the simulated and analytically estimated (Eq. (5.1)) numbers of contacts per fiber N_c. The simulation result is for the structure that appears at the maximal force of the stress-strain curve. Low and basic refer to a network of low grammage and the basic network, respectively. Different points for a given network grammage correspond to networks with varying fiber stiffness (k_b = 50 - 5000) or adhesion force (F_{ad} = 25 - 1000).

The above estimates can be compared with simulated numbers of contacts per fiber, $N_c^{simu\_2D}$, determined by projecting the network onto the xy plane. The ratio of contact numbers of unloaded to deformed networks is $N_c^{simu\_2D} / N_c^{simu\_2D\_\max} = 0.85$, which compares nicely with the ratio of the effective areas. Moreover, this analysis suggests that for very low grammage (8 g/m^2) and flexible fibers (k_b = 50), the number of contacts per fiber may even increase during straining due to the decreased effective sheet area. In addition, in Fig. 18 we also plot the number of simulated fiber-fiber contacts, which increases by a factor of 1.6 during straining.

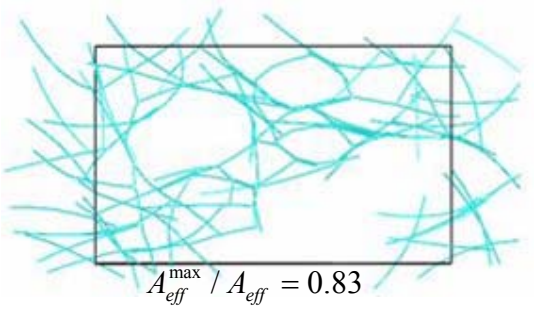

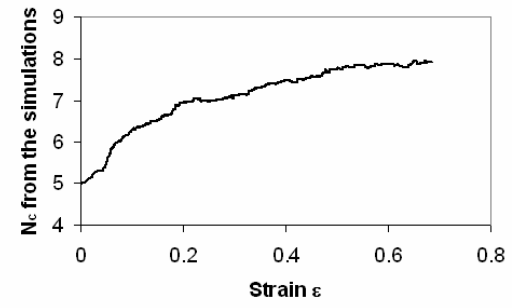

Figure 18. Top view of a fiber network after loading to the maximum force, and a simulated number of contacts per fiber as a function of strain for a network of low grammage, an adhesion force of F_{ad} = 1000, and a fiber stiffness of k_b = 50. The effective sheet area A_{eff} is only 17% of the total area. The ratio of

the effective areas of deformed and unloaded networks is 83 %, and the ratio of the simulated fiber-fiber contacts projected onto the xy plane of the unloaded and deformed networks is 85 %.

5.2 In-plane deformations

For fiber networks with no periodic boundary conditions in the y direction, lateral contraction is determined as $\varepsilon_y = \Delta y/L_{yo}$, where $\Delta y = \Delta y_+ + \Delta y_-$ is the sum of the average lateral displacements of the fiber segments that initially intersect the planes at $y = \pm mL/2$ (m= 6 in the simulations discussed here), L_{yo} is the initial network width, and L_x is the initial gap, c.f. Fig. 19. The Poisson ratio for the lateral contraction is defined as $\nu_{xy} = -\varepsilon_y / \varepsilon_x$.

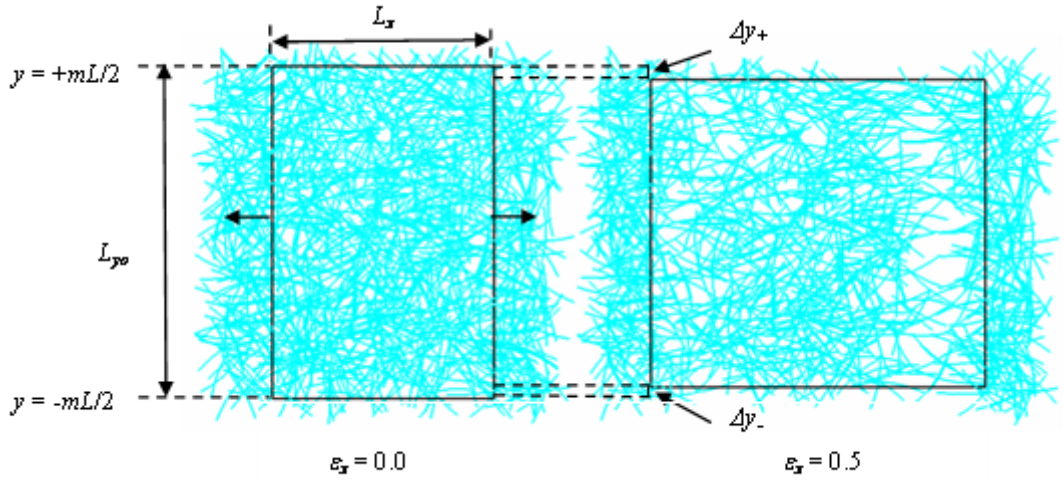

Figure 19. A typical fiber network with no periodic boundary conditions in the y direction at strains ε_x = 0.0 and 0.5. L_{y0} is the initial width, L_x is the gap length, and Δy is the sum of the average lateral displacements of the fiber segments that initially intersect the planes at $y = \pm mL/2$.

In Fig. 20a we show the transverse strain ε_y as a function of strain ε_x for various gap lengths L_x and the sample width $L_y = 6L$. We used only one initial fiber network for all other gap lengths except for $L_x = 4L$. For this largest gap length, we performed simulations on four additional replicate networks for comparison. In general, the lateral contraction increased systematically with increasing gap length as the deformations were less restricted by the boundary conditions at the gap ends. The data of Fig. 20a can be used to determine the Poisson ratio for the deformation in the lateral direction, ν_{xy}, shown in Fig. 20b. This ratio increases with increasing applied strain, ε_x, and reaches a constant value in the range ν_{xy} = 0.05 – 0.16 before the network rupture. The increase of Poisson ratio is in contrast to earlier findings by Habeger (1985) for dry paper. On the other hand, the plateau corresponds to a slow rupture process of the network during which changes in the lateral Poisson ratio are very small. It is difficult to pinpoint an exact strain value for network failure as there are large force fluctuations near the maximum force. For this reason, the end points of

the curves vary a lot depending on the gap length. The model of Ramasubramanian and Perkins (1988) was more advanced, and they were able to incorporate the complex and inelastic behavior of bonds and fibers. They showed that the lateral contraction ratio decreases or increases with increasing applied strain when network is strained beyond the elastic region. However, for small enough strains the in-plane Poisson ratio is always constant as found experimentally by Göttsching and Baumgarten (1976) for dry paper.

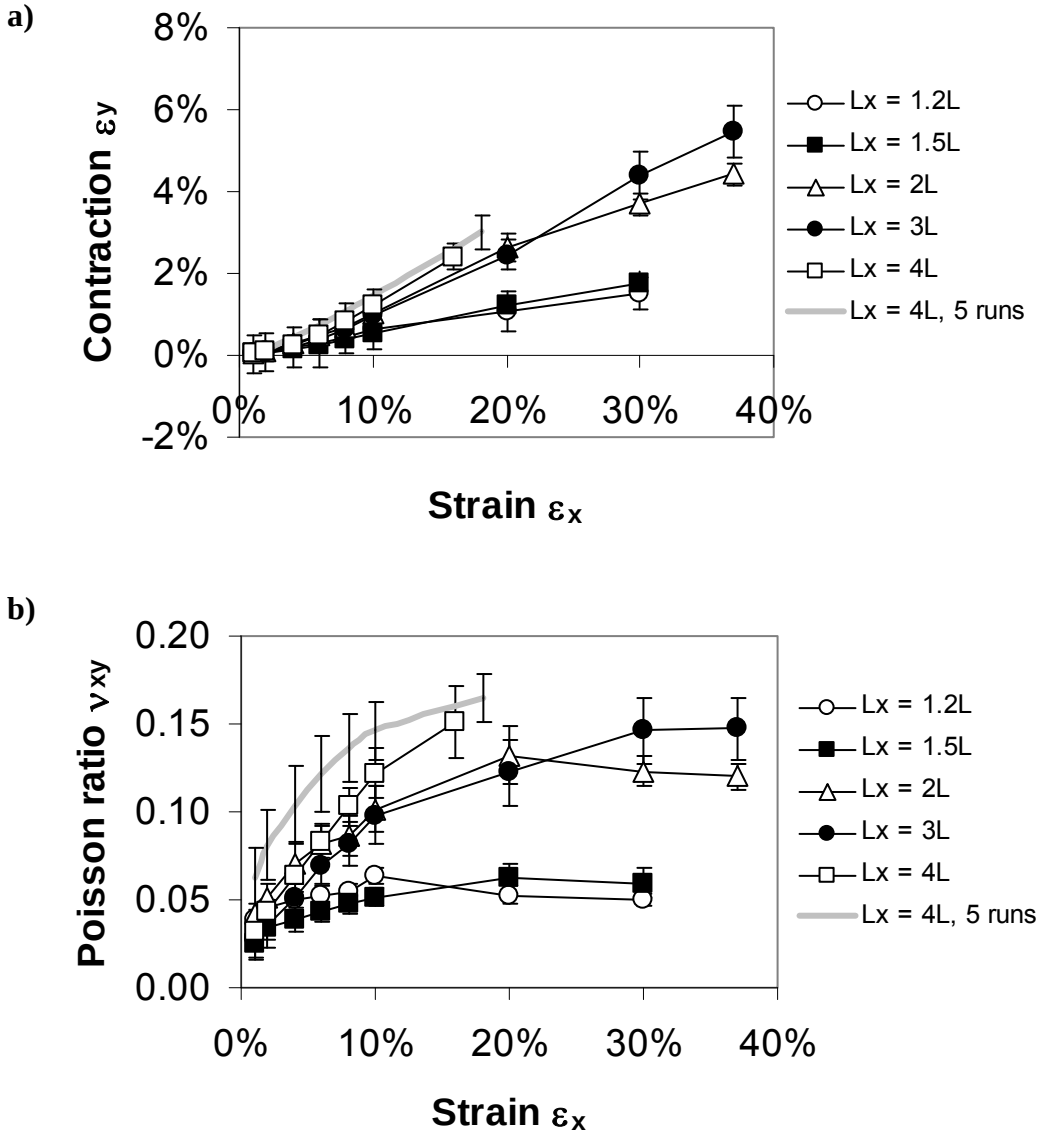

Figure 20. a) Network contraction in the lateral direction (ε_y) and b) the corresponding Poisson ratio (ν_{xy}) as a function of strain ε_x up to the point of maximum tensile force for the gaps L_x/L = 1.2, 1.5, 2.0, 3.0, and 4.0. The network width is $L_y = 6L$, adhesion force is $F_{ad} = 25$, and fiber stiffness is k_b = 50. Grey solid curves show the average of five replicate networks for L_x/L = 4.0 with a 95% confidence limit. In the case of only one simulated network, the error bars indicate the uncertainty in the estimated lateral contraction.

5.3 Deformations in the thickness direction

The strain in the thickness direction is defined as $\varepsilon_z = (h-h_o)/h_o$, where h_o is the initial network (Fig. 14) thickness and h is the network thickness at strain ε_x. The Poisson ratio for expansion in the thickness direction is defined as $\nu_{xz} = -\varepsilon_z/\varepsilon_x$. Contraction in the thickness direction is not restricted by the boundary conditions at the gap ends. Therefore, we do not expect network contraction in the thickness direction to depend at all on the gap length L_x. The thickness contraction data of Fig. 21a (black solid line) indeed appears to follow roughly the same quadratic curve for all gap lengths,

$$\varepsilon_z = c_1\varepsilon_x^2 + c_2\varepsilon_x, \tag{5.2}$$

with the parameters c_1 = -0.35 and c_2 = 0.32. A quadratic thickness reduction implies a linear behavior for the Poisson ratio ν_{xz} in Fig. 21b (black solid line). Due to the very large deviations in ν_{xz} at small elongations, it would be hard to argue based solely on Fig. 21b that ν_{xz} slightly decreases with increasing elongation ε_x. The original contraction data of Fig. 21a are needed to draw this conclusion.

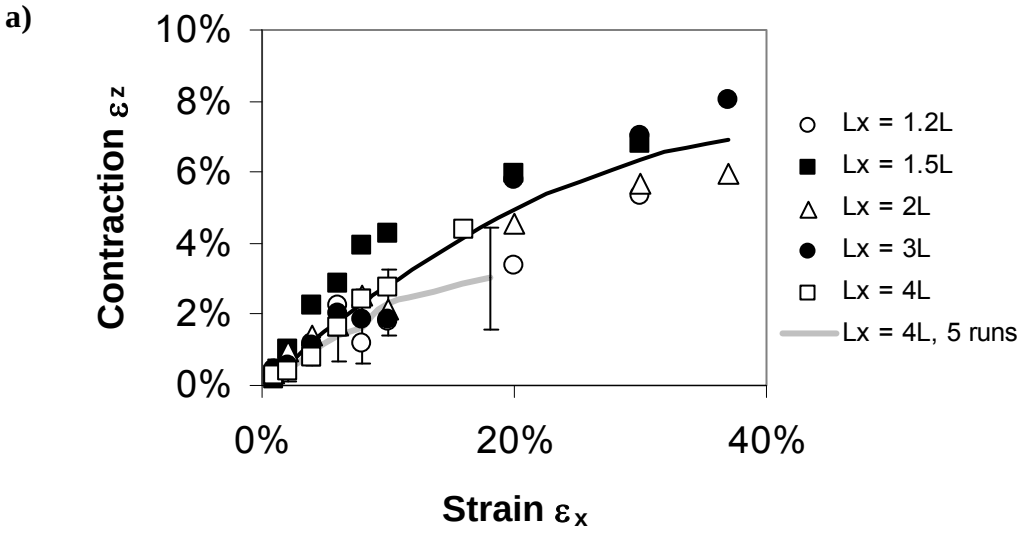

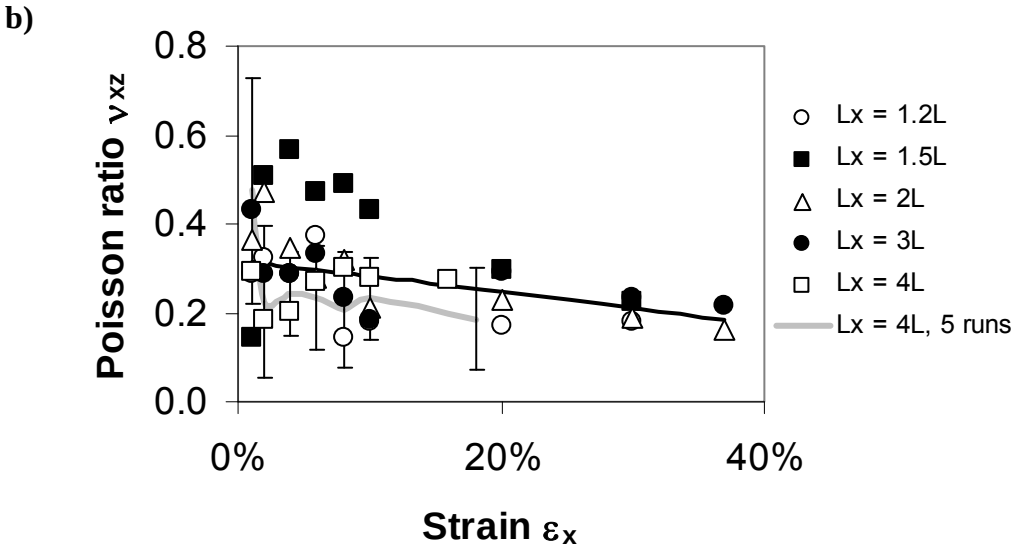

Figure 21. a) Network contraction in the thickness direction (ε_z) and b) the corresponding Poisson ratio (ν_{xz}) as a function of strain ε_x up to the point of maximum tensile force for the gaps L_x/L = 1.2, 1.5, 2.0, 3.0, and 4.0. The network width is $L_y = 6L$, adhesion force is $F_{ad} = 25$, and fiber stiffness is $k_b = 50$. The grey solid curves show the average of five replicate networks for $L_x/L = 4.0$ with a 95% confidence limit. In Fig. a) the black curve shows the quadratic prediction for ε_z and in Fig. b) it shows the linear prediction for ν_{xz}.

Deformations in the thickness direction increase with increasing adhesion force as shown in Fig. 22a. Equation (5.2) is plotted in Fig. 22a as a dashed line for the adhesion force $F_{ad} = 25$, and as a solid line for the adhesion force $F_{ad} = 250$ ($c_1 = -1.18$ and $c_2 = 0.63$). Similar curves for the Poisson ratio in the thickness direction are shown in Fig. 22b. The effect of adhesion force on the Poisson ratio is significant. However, the general trends are very similar for both adhesion levels.

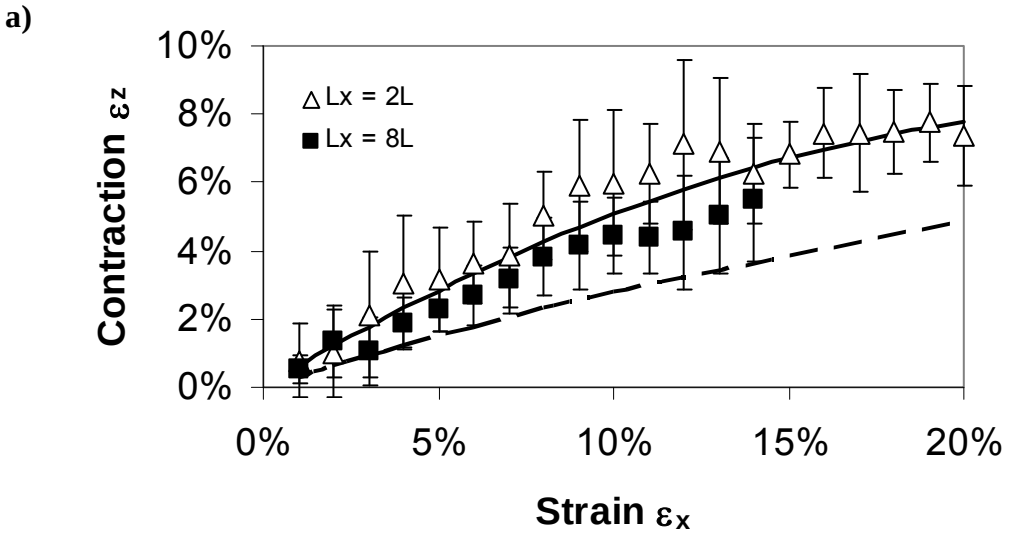

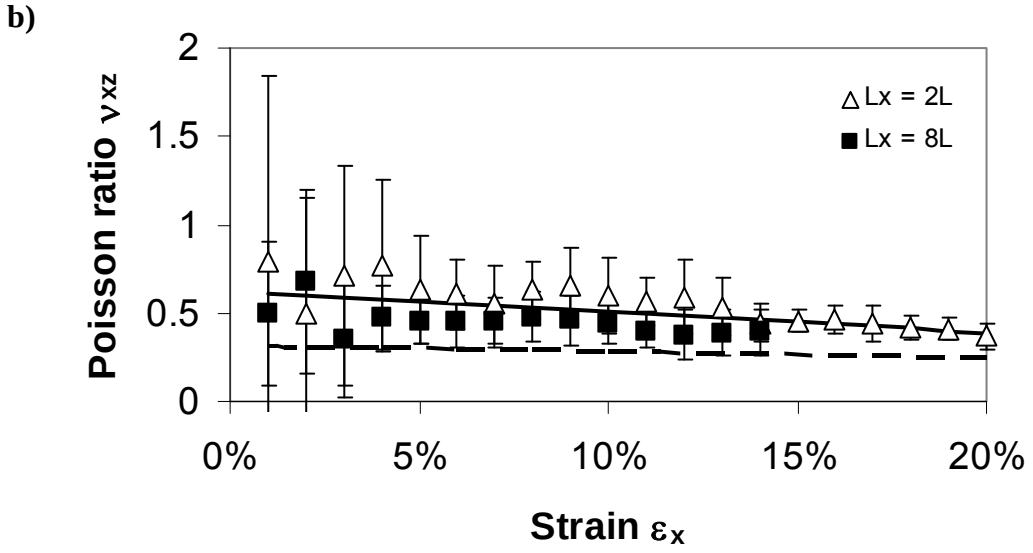

Figure 22. a) Network strain in the thickness direction (ε_z) and b) the corresponding Poisson ratio (ν_{xz}) as a function of strain ε_x up to the point of maximum tensile force for the gaps L_x/L = 2.0 and 8.0. The network width is L_y = 2L, adhesion force is F_{ad} = 250, and fiber stiffness is k_b = 50. Results are averages of six replicate networks with 95% confidence. We also show a) a quadratic and b) a linear behavior for F_{ad} = 250 (solid line), and compare it with a similar prediction (obtained from Fig. 21) for F_{ad} = 25 (dashed line). Periodic boundary conditions in both the x and y directions were used in the simulations for the higher adhesion level.

Network strain in the thickness direction for varying fiber stiffness k_b is shown in Fig. 23. Göttsching and Baumgarten (1976) studied extensively triaxial deformations under tensile load in different paper grades. Assuming that increased beating increases fiber flexibility (decreases fiber stiffness), we were able to reproduce their findings. They found that for low beating, the network thickness may increase during stretching and can eventually exceed the original thickness close to the strain at break. This corresponds to our simulation result for stiff fibers (k_b = 500.0), for which the network thickness slightly increases for some fiber networks during straining. Also Stenberg and Fellers (2002) found thickness to increase during in-plane tensile loading in some of their experiments, but at the same time they recognized that thickness may also decrease as our simulations indicate. In addition, thickness increase was also suggested by Öhrn (1965) for dry papers and by simulations (Åström et al. 2000b) for fiber networks of rigidly bonded fibers. Even though the above experimental results were for *dry* papers, an analogous behavior may be observed in *wet* papers (Baum et al. 1984). The rate of thickness decrease during stretching is faster for flexible (increased beating) than stiff fibers as shown in Fig. 23. However, experiments on oriented sheets confirm a systematic increase in the thickness (Göttsching and Baumgarten 1976; Baum et al. 1984; Stenberg and Fellers 2002).

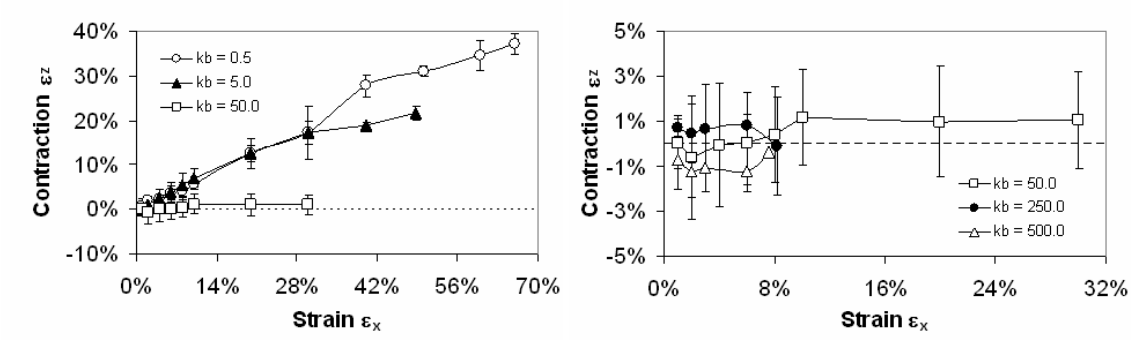

Figure 23. Network strain in the thickness direction (ε_z) as a function of strain ε_x for the fiber stiffnesses k_b = 0.5, 5.0, and 50.0 (on the left), and for the fiber stiffnesses k_b = 50, 250, and 500.0 (on the right) during mechanical testing up to the point of average strain at break. Results are averages of three simulations. The error bars indicate the standard deviation.

Snapshot side views of deformed networks are plotted in Fig. 24 for very flexible (k_b = 0.5) and stiff fibers (k_b = 500.0). These plots clearly confirm that a network of stiff fibers deforms much less during straining both in the straining and thickness directions than that of flexible fibers.

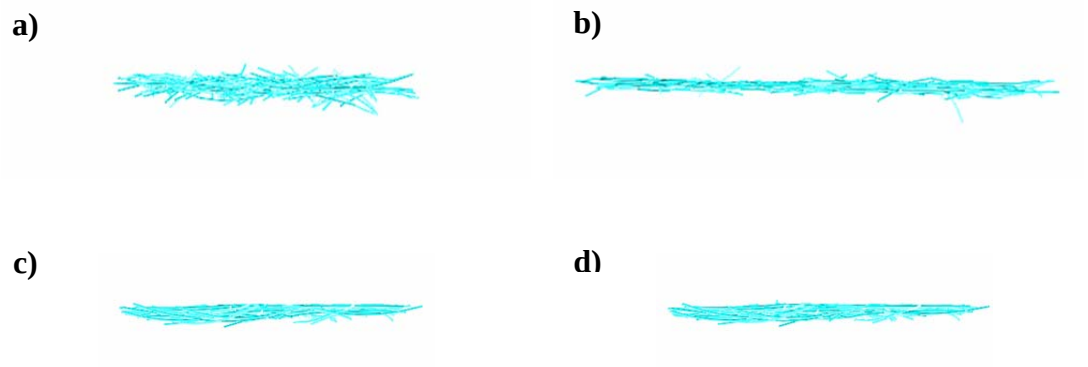

Figure 24. Snapshot side views of fiber networks for a) the fiber stiffness k_b = 0.5 and no strain, b) the fiber stiffness k_b = 0.5 and the strain at failure ε_{max} = 0.8, c) fiber stiffness k_b = 500.0 and no strain, and d) fiber stiffness k_b = 500.0 and the strain at failure ε_{max} = 0.08. In all cases the adhesion force was F_{ad} = 25.

Chapter 6

6 Conclusions

Simulations of wet fiber networks can be used to predict tensile strength and stiffness. The tensile strength results are described surprisingly well by a simple model with the adhesion force, number of inter-fiber contacts, friction, and network grammage as the key parameters. The strength appears rather insensitive to network structure, sample size, and fiber stiffness for a given network grammage, density, adhesion force and friction.

Simulated relaxation of tensile force in wet fiber networks compares well with experimental results for wet and dry paper, and the force decreases proportional to logarithmic time. Relaxation rate for simulated wet web and wet paper was faster than for dry paper whose properties are known from earlier experiments. Simulated networks displayed strain recovery under relaxation, which was much smaller than in experiments on real wet paper. Complete lack of bonding or the description used for the interaction between wet fibers in the simulation model could at least partially explain this difference. To this end the nature of adhesion forces between wet fibers should be analyzed in more detail experimentally.

Understanding the factors that affect the structure of fiber networks will increase our knowledge of their mechanical properties. One of the most important factors that describe the network structure is the number of inter-fiber contacts. We compared analytical estimates for this number (Corte and Kallmes 1962, Komori and Makishima 1977) to our computer simulations for compressed and stretched fiber networks. The analytical results were based on the fiber diameter, number of fibers in a given volume, and fiber length. They worked very well for closely isotropic fiber networks with high enough network density. Estimation of sheet thickness was hampered by surface roughness.

Deviations from analytical estimates were observed in simulations for stretched flocculated sheets, where the effective sheet area related to strength can be much smaller than the total sheet area. This finding confirms that mean-field models cannot work for wet fiber networks with flocculated fibers since the flocs remained mainly intact during straining, and the network strain was concentrated between flocs. On the other hand, our theoretical analysis suggested that the effect of fiber orientation on the number of inter-fiber contacts is rather small for networks of practical interest. Also, no significant effect in stretched networks arose from simulations with inhomogeneous orientation distributions.

Numerical studies showed that the lateral Poisson ratio depends on the applied strain as also shown by earlier micromechanical models. According to our simulations, boundary conditions at the gap edges become increasingly important when the gap is made shorter. In the thickness direction the fiber network usually contracted as found experimentally for isotropic sheets, but the magnitude of contraction depended on fiber stiffness. However, for very stiff fibers the network thickness may also increase

as proposed earlier for wet paper. In addition, experiments on oriented sheets display a systematic increase in the thickness.

Effects of distributions of fiber properties should be studied further in order to better describe realistic wet paper. The biggest experimental challenges will be related to systematic variation of structural and fiber properties, together with their characterization, and to characterization of fiber-fiber interactions. New experimental techniques will probably be needed.

Changes in network dimensions during straining are related to changes in the network porosity. In the simulations discussed here, porosity increased only slightly during stretching due to its large initial value (> 0.90). Simulations with more realistic network porosities (0.29 – 0.87 (Yamauchi et al. 1975; Yamauchi, Kibblewhite 1988)) would probably result in larger changes in porosity during straining.

The simulation model and methods along with the results presented here can be applied to materials that can be considered as networks of non-bonded elongated particles. In this work, elongated fibers were composed of rigid segments that deformed by bending and twisting only. This kind of behavior should be rather typical of slender elongated particles in particular.

Bibliography

Batchelor, W.J, and Westerlind, B.S. (2003): Measurement of short span stress-strain curves of paper, Nord. Pulp Pap. Res. J 18(1), 44.

Baum, G.A., Pers, K., Shepard, D.R. and Ave'Lallemant, T.R. (1984): Wet straining of paper, Tappi J. 67(5), 100.

Campbell, W.B. (1959): The Mechanism of Bonding, Tappi J. 42(12), 999.

Corte, H. and Kallmes, O.J. (1962): Statistical Geometry of a Fibrous Network, ed. by Bolam, F., Formation and Structure of Paper, September 1961, Trans Fund. Res. Sym., Oxford, 1962, pp. 13-46.

Cox, H.L. (1952): The elasticity and strength of paper and other fibrous materials. British Journal of Applied Physics, 72(3).

Craven, B.D. (1962): Stress relaxation and Work Hardening in Paper, Appita 16(2), 57.

Dodson, C.T.J. and Deng, M. (1994): Paper: An Engineered Stochastic Structure. Tappi Press, Atlanta.

Duncker, B., Hartler, N., and Samuelson, L.G. (1965): Effect of Drying on the Mechanical Properties of Pulp Fines,, Trans. IIIrd. Fund. Res Symp. Cambridge, pp 529-537, FRC.

Göttsching, L. and Baumgarten, H.L. (1976): Triaxial Deformation of Paper Under Tensile Load, ed. by Bolam, F., The Fundamental Properties of Paper Related to its Uses, London, pp 227-249.

Habeger, C.C. (1985): An Addition to the Seth-Page Nonlinear Network Model for Paper, J. Pulp Paper Sci. 11(2), J51.

He, J., Batchelor, W.J. and Johnston, R.E. (2003): An Analytical Model for Number of Fibre-Fibre Contacts in Paper and Expressions for Relative Bonded Area (RBA), Preprint of 2003 Int. Paper Physics Conf, Victoria, BC, Canada, September 7-11, 2003.

Heyden, S. (2000): Network Modelling for the Evaluation of Mechanical Properties of Cellulose Fluff, Ph.D. Thesis, Lund University, Lund.

Htun, M., and de Ruvo, A. (1977): Relation between drying stresses and internal stresses and the mechanical properties of paper, Trans. VIth Fund. Res. Symp. Oxford, pp 477–487, FRC.

Jantunen, J. (1985): Visco-Elastic Properties of Wet Webs under Dynamic Conditions, Transactions of The 8th Fundamental Research Symposium held at Oxford, 1985, Mechanical Engineering Publications Ltd, London, pp. 133-162.

Johanson, F, and Kubat, J. (1964): Measurements of Stress Relaxation in Paper, Svensk Papperstid 67(20), 822.

Kallmes, O.J., and Perez, M. (1965): Load/Elongation properties of fibres, Trans. IIIrd. Fund. Res Symp. Cambridge, pp 507-528, FRC.
Komori, T. and Makishima, K. (1977): Number of Fiber-to-Fiber Contacts in General Fiber Assemblies, Textile Res. J. 47, 13.
Kouko, J., Salminen, K., and Kurki, M. (2007): Laboratory scale measurement procedure for the runnability of a wet web on a paper machine, Part 2, Paperi ja Puu, 89(7-8), 424.
Kurki, M., Kekko, P., Kouko J. and Saari T. (2004): Laboratory scale measurement procedure of paper machine wet web runnability. Part 1, Paperi ja Puu 86(4), 256.
Lindström, S. B. (2008): Modelling and Simulation of Paper Structure Development, Ph.D. Thesis, Mid Sweden University, Sundsvall.
Lyne, L.M. and Gallay, W. (1954a): Measurement of Wet Web Strength, Tappi J. 37(12), 694.
Lyne, L.M. and Gallay, W. (1954b): Studies in the Fundamentals of Wet Web Strength, Tappi J. 37(12), 698.
Lyne, L.M. and Gallay, W. (1954c): Fiber Properties and Fiber-Water Relationships in Relation to the Strength and Rheology of Wet Webs, Tappi J. 37(12), 581.
Makela, P. (2007): The Effect of Moisture Ratio and Drying Restraint on the Stress Relaxation of Paper In: Proceedings: 61st Appita Annual Conference and Exhibition, Gold Coast, Australia 6-9 April 2007; pages: 169-177. Carlton, Vic.: Appita Inc., 2007.
Mäkinen, J. (2001): The mechanical and geometrical properties of fibrous structures, Ph.D. Thesis, University of Jyväskylä, Jyväskylä, Finland.
Niskanen, K. (1998): Paper Physics. Papermaking Science and Technology, Book 16. Finnish Paper Engineers' Association and TAPPI, Finland, 1998.
Page, D.H., Seth, R.S. and De Grace, J.H. (1979): The elastic modulus of paper, Tappi J. 62(9), 99.
Page, D.H.(1993) :A Quantative Theory of the Strength of Wet Webs, J. Pulp. Paper, Sci., 19(4), 175.
Page, D.H., and Seth, R.S. (1980): The elastic modulus of paper, Tappi J. 63(6), 113 and 63(10), 99.
Page, D.H and Tydeman, P.A. (1965): Physical Processes Occurring during the Drying Phase, Trans. IIIrd. Fund. Res Symp. Cambridge, pp 371-396., FRC.
Ramasubramanian, M.K. (1987): Computer Simulation of the Uni-axial Stress-strain Behavior of Ribbon-like Fiber Nonwovens, Ph.D. Thesis, Syracuse University.
Ramasubramanian, M.K. and Perkins, R.W. (1988): Computer Simulation of the Uniaxial Elastic-Plastic Behavior of Paper, J. of Engineering Materials and Technology 110, 117.

Robertson, A.A. (1963): The Physical Properties of Wet Webs, Part 2. Fibre Properties and Wet Web Behaviour, 66(12), 477-497.
Salmén, L., Boman, R., Fellers, C., and Htun, M. (1987): The implications of fiber and sheet structure for the hygroexpansivity of paper, Nordic Pulp and Paper Research Journal, 2(4), pp 127-131.
Sampson, W.W. (2001): The Structural Characterisation of Fibre Networks in Papermaking Processes – A Review, ed. by Baker, C.F., The science of papermaking, Transactions, XIIth Fundamental Research Symposium, September 2001, Pulp and Paper Fundamental Research Society, Bury, pp. 1205-1288.
Schmid, C.F., Switzer, L.H. and Klingenberg, D.J. (2000): Simulations of fiber flocculations: effects of fiber properties and interfiber friction, J. Rheol. 44(4), 781.
Seth, R.S. and Page, D.H. (1983): The Stress-strain Curve of Paper, ed by J. Brander, The Role of Fundamental Research in Paper Making, Mechanical Engineering Publ., Ltd., London, 421.
Seth, R.S. (1995): The effect of fiber length and coarseness on the tensile strength of wet webs: a statistical geometry explanation, Tappi J., 78(3), 99.
Shallhorn, P.M. (2002): Effect of Moisture Content on Wet-Web Tensile Properties, J. Pulp. Paper, Sci., 28(11), 384.
Stenberg, N. and Fellers, C. (2002): Out-of-plane Poisson's ratios of paper and paperboard, Nord. Pulp Pap. Res. J 17(4), 387.
Switzer III, L. H. (2002): Simulating Systems of Flexible Fibers, Ph.D. Thesis, University of Wisconsin-Madison, Madison, WI.
Switzer, L.H. and Klingenberg, D.J. (2003): Simulations of fiber floc dispersion in linear flow fields, Nord. Pulp Pap. Res. J 18(2), 141.
Switzer, L.H., Klingenberg, D.J. and Scott, C.T. (2004): Handsheet formation and mechanical testing via fiber-level simulations, Nord. Pulp Pap. Res. J 19(4), 434.
Yamauchi, T., Murakami, K. and Imamura, R. (1975): The Porous Structure of Paper, Analytical Research on the Behavior of Mercury Penetration and Retraction, Jpn. Tappi 29(9), 492.
Yamauchi, T. and Kibblewhite, R.P. (1988): Pore Structure of Paper Webs from Radiata Pine Thermomechanical Pulp, Appita J. 41(1), 37.
Åström, J.A., Mäkinen, J.P., Alava, M.J., and Timonen, J. (2000a): Elasticity of Poissonian fiber networks, Phys. Rev. E 61, 61(5), 5550; Phys. Rev. E 62(4), 5862.
Åström, J.A., Mäkinen, J.P., Hirvonen, H., and Timonen, J. (2000b): Stiffness of compressed fiber mats, J. Appl. Phys. 88(9), 5056.
Åström, J.A., Latva-Kokko, M., Kähkönen, S., Mäkinen, J.P., and Timonen, J. (2003): The role of connectivity in the properties of sedimented materials, Granular Matter 5, 99.
Öhrn, O.E. (1965): Thickness Variations of Paper on Stretching, Svensk Papperstidn. 68(5), 141.